P10.15 NUMERICAL SIMULATION OF LOW-LEVEL MISOCYCLONES ASSOCIATED WITH WINTER CONVECTIVE CELLS: A CASE STUDY FROM THE SHONAI AREA RAILROAD WEATHER PROJECT

Ken-ichi Shimose[1*], Syugo Hayashi[2], Wataru Mashiko[2], Kenichi Kusunoki[2], Kotaro Bessho[3], Shunsuke Hoshino[2], Keiji Araki[4], Hanako Inoue[2], Masahisa Nakazato[2], Yoshihiro Hono[5], Toshiaki Imai[4], Keiji Adachi[5], Hiroshi Yamauchi[2], and Tetsuya Takemi[6]

[1]Alpha-denshi Co., Ltd. / Meteorological Research Institute, Japan, [2]Meteorological Research Institute, Japan, [3]Japan Meteorological Agency, Japan, [4]Railway Technical Research Institute, Japan, [5]East Japan Railway Company, Japan, [6]Kyoto University, Japan

1. INTRODUCTION

In order to develop an automatic strong gust detection system for railroad, the Shonai area railroad weather project has investigated the property of wind gust using two X-band Doppler radars and the network of 26 surface weather stations since 2007 (see Fig. 1 for their locations). Through the project, we understand the aspect of wind gust. The remarkable result is that observed gusts are mainly associated with low-level misocyclones. Simultaneously, we find problems to be solved. In particular, it is difficult to capture the near-surface structure of wind gust by the radar. Thus, a numerical approach is effective in compensating near-surface information.

This study describes the numerically simulated structure of low-level misocyclones, one of which generated observed wind gust, associated with winter convective cells observed at 11 December 2008. Fortunately, for this case, the damage has not been reported.

2. CASE OVERVIEW

The gust was observed at the Sakata meteorological observatory (see Fig. 1 for its location). The maximum wind speed was 26.8 m s^{-1} at 1711 JST (Japan Standard Time: UTC + 9 hours).

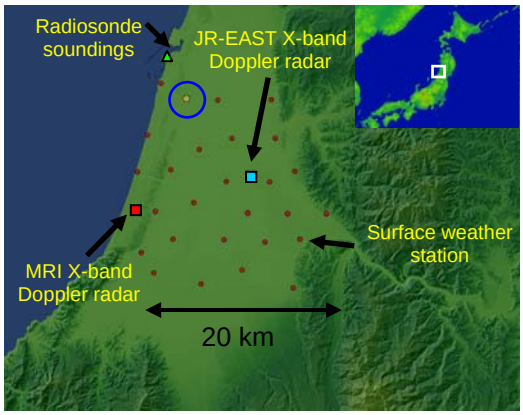

Figure 1: Map of the Shonai area. The locations marked by the symbols are as follows: the network of automated weather station sites (red circles), Sakata meteorological observatory (open circle), the X-band Doppler radar sites of MRI radar (red square) and JR-EAST radar (water square), and radiosonde soundings (triangle). The inset shows the locations of the Sea of Japan and the study area (in the square).

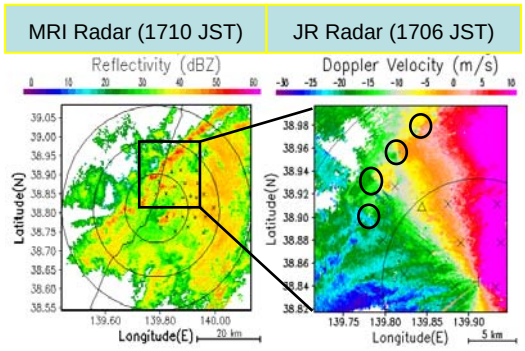

Figure 2: (Left) Radar reflectivity field from MRI radar. Costal line is denoted by thin line. (Right) Doppler velocity field from JR radar. Inside of the open square in the left panel is shown. Open circles indicate the vortex pattern.

In this case, convective cells were initiated along the cold front over the sea (not shown). Figure 2 shows the radar reflectivity and Doppler velocity fields from two Doppler radars. Misocyclones were

* *Corresponding author address:* Ken-ichi Shimose, Meteorological Research Institute, 1-1 Nagamine, Tsukuba, Ibaraki 305-0052, Japan; e-mail: kshimose@mri-jma.go.jp

distributed at 2-4 km intervals and some of them landed. Misocyclones were embedded in the surface convergence line (not show).

3. NUMERICAL MODEL

The nonhydrostatic numerical model, JMANHM (Saito et al. 2006), is used to simulate the misocyclones. The model is initialized by MANAL, which data is an objective analysis made by the Japan Meteorological Agency and horizontal resolution is 10 km. No special observed data is assimilated in this case. The finest horizontal grid spacing is 250 m.

4. RESULTS

The model succeeds in simulating convective cells and misocyclones along the surface convergence line. Figure 3 shows the three-dimensional view of simulated misocyclone at 1710 JST. The height of misocyclone top is about 2 km. Simulated misocyclones are distributed at 2-5 km intervals. These intervals are similar to observed intervals.

To investigate the development process of misocyclones, the evolution of the maximum vorticity of the representative misocyclone is calculated. Figure 4 shows the time-height cross-section of the maximum vertical vorticity of the representative misocyclone. The simulated misocyclone is initiated below the height of 500 m, where the horizontal convergence is significantly strong. There is no upper signal when the misocyclone starts to develop. Then the misocyclone extends upward and reaches the height of 2 km. These simulated structure and evolution of misocyclones are similar to the results of Lee and Wilhelmson (1997a, b).

The structure of the misocyclone changes in the vicinity of the landfall. Figure 5 shows the vertical cross-sections of the vertical vorticity across the center of the representative misocyclone. After the landfall, the vertical structure of the misocyclone greatly tilts to the advected direction.

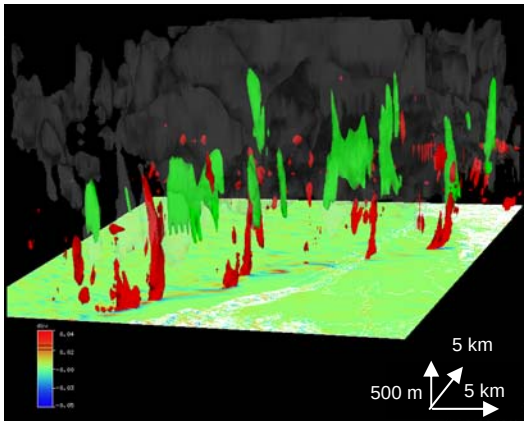

Figure 3: 3D view of simulated misocyclones at 1710 JST. Iso-surfaces are indicated as follows: vertical vorticity (> 0.02 s^{-1}, red), updraft (> 5 m s^{-1}, green) and condensate (> 0.2 g kg^{-1}, gray). Surface color and contour denote the divergence field and elevation height, respectively.

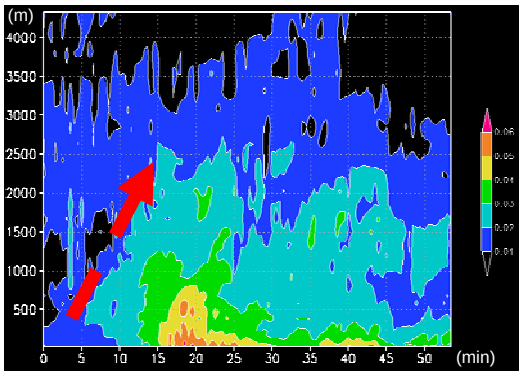

Figure 4: Time-height cross-section of the maximum vertical vorticity of the representative vortex.

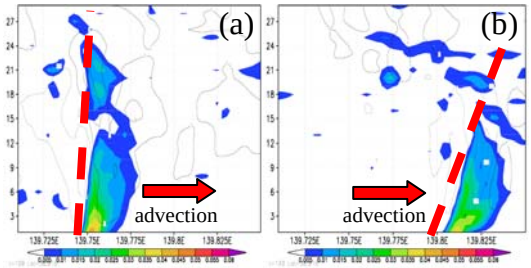

Figure 5: Vertical cross-sections of the vertical vorticity across the center of the representative vortex. (a) before landfall, (b) after landfall.

5. FUTERE WORK

The initial development of the miso-cyclone starts at the height of 500 m with no upper signal. Furthermore, the structure of the misocyclone changes in the vicinity of the landfall. It is necessary for the radar

scan to monitor the lower layer (below 1 km height) frequently. We have to take into account the change of the structure in the vicinity of the landfall.

ACKNOWLEDGEMENTS

This work was supported by the Program for Promoting Fundamental Transport Technology Research from the Japan Railway Construction, Transport and Technology Agency (JRTT).

REFERENCES

Lee, B.D., and R.B. Wilhelmson, 1997a: The numerical simulation of non-supercell tornadogenesis. Part I: Initiation and evolution of pre-tornadic misocyclone circulations along a dry outflow boundary. *J. Atmos. Sci.,* **54,** 32 – 60.

Lee, B.D., and R.B. Wilhelmson, 1997b: The numerical simulation of non-supercell tornadogenesis. Part II: Evolution of a family of tornadoes along a weak outflow boundary. *J. Atmos. Sci.,* **54,** 2387 – 2415.

Saito, K., and Coauthors, 2006: The operational JMA nonhydrostatic mesoscale model. *Mon. Wea. Rev.*, **118**, 891-917.